

Water Resources Research



RESEARCH ARTICLE

10.1029/2023WR036090

Key Points:

- The erosion-deposition propagation of debris flow is confirmed by surgedepth hydrographs measured at the Jiangjia Ravine, Yunnan Province, China
- Shallow and deep erosion patterns are revealed by hydraulic jump equations.
 The debris-flow surges at the Jiangjia Ravine fall into the deep erosion
- The destructiveness of debris-flow surges is quantified by considering the momentum hidden under the surge front and confirmed by field observation

Supporting Information:

Supporting Information may be found in the online version of this article.

Correspondence to:

D. Song, drsong@imde.ac.cn

Citation:

Chen, Q., Song, D., Chen, X., Feng, L., Li, X., Zhao, W., & Zhang, Y. (2024). The erosion pattern and hidden momentum in debris-flow surges revealed by simple hydraulic jump equations. *Water Resources Research*, 60, e2023WR036090. https://doi.org/10.1029/2023WR036090

Received 21 AUG 2023 Accepted 29 OCT 2024

Author Contributions:

Conceptualization: Qian Chen,
Dongri Song
Data curation: Xiaoyu Li
Formal analysis: Qian Chen, Lei Feng
Funding acquisition: Dongri Song,
Xiaoqing Chen, Wei Zhao, Yaonan Zhang
Investigation: Qian Chen, Xiaoyu Li
Methodology: Qian Chen, Dongri Song
Project administration: Xiaoqing Chen,
Wei Zhao, Yaonan Zhang
Supervision: Dongri Song, Yaonan Zhang
Validation: Qian Chen, Lei Feng

© 2024. The Author(s). This is an open access article under the terms of the Creative Commons Attribution License, which permits use, distribution and reproduction in any medium, provided the original work is properly cited.

Writing - original draft: Qian Chen

The Erosion Pattern and Hidden Momentum in Debris-Flow Surges Revealed by Simple Hydraulic Jump Equations

Qian Chen^{1,2}, Dongri Song^{1,2,3}, Xiaoqing Chen^{1,2}, Lei Feng^{1,2}, Xiaoyu Li¹, Wei Zhao^{1,2}, and Yaonan Zhang^{3,4}

¹Institute of Mountain Hazards and Environment, Chinese Academy of Sciences, Chengdu, China, ²University of Chinese Academy of Sciences, Beijing, China, ³National Cryosphere Desert Data Center, Lanzhou, China, ⁴Northwest Institute of Eco-Environment and Resources, Chinese Academy of Sciences, Lanzhou, China

Abstract The erosion-deposition propagation of granular avalanches is prevalent and may increase their destructiveness. However, this process has rarely been reported for debris flows on gentle slopes, and the contribution of momentum hidden under the surge front to debris-flow destructiveness is ambiguous. Therefore, the momentum carried by the apparent surge front is often used to indicate debris-flow destructiveness. In this study, the erosion-deposition propagation is confirmed by surge-depth hydrographs measured at the Jiangjia Ravine (Yunnan Province, China). Based on simple hydraulic jump equations, the eroded deposition depth of surge flow is quantified, and the erosion pattern can be divided into two patterns (shallow and deep erosion). For surge flows with erosion-deposition propagation, significant downward erosion potential is confirmed, and debris-flow surge erosion is considered the deep erosion. The total momentum carried by surge flow is further quantified by two Froude numbers (surge-front and rearward Froude numbers) and verified through the field observation of surge flows. The total momentum of surge flow not only originates from the apparent surge front, but also includes the momentum within the eroded deposition layer. This study provides a theoretical approach for quantifying the upper limit of erosion depth and revealing the destructiveness of debris-flow surges. A perspective on the importance of substrate deposition for debris-flow erosion on gentle slopes is emphasized, as this approach can improve the reliability of debris-flow risk assessment.

Plain Language Summary For flow-type mass movements consisting of multiple surges, a subsequent surge would entrain the deposition of previous surges. The subsequent surge continues to move forward until it deposits again. This deposition is in turn carried away by the subsequent surges. This process is termed erosion-deposition propagation. The erosion-deposition propagation widely occurs in snow avalanches and enhances destructiveness by amplifying the scale and mobility of avalanches. For debris flows on gentle slopes, erosion-deposition propagation has not been reported, and the effect of this process on debris-flow destructiveness is unclear. In this study, the erosion-deposition propagation of debris flows is confirmed by the field observation of surge flows at the Jiangjia Ravine (Yunnan Province, China). Based on simple hydraulic jump equations, the erosion into deposition of surge flow is quantified. The erosion patterns and momentum hidden under debris-flow surges are revealed. The deep erosion pattern means that the apparent debris-flow surge is merely "the tip of the iceberg," and there is a large portion underneath. This study proposes a theoretical approach for quantifying the eroded deposition depth and the total momentum carried by debris-flow surges, which is conducive to a precise risk assessment and mitigation of debris-flow surges.

1. Introduction

For destructive flow-type mass movements, material masses generally do not flow continuously along paths but develop into series of surges (Comiti et al., 2014; Major et al., 2005; McArdell et al., 2007; Sovilla & Bartelt, 2002). This multiple-surge propagation is very common in debris flows (Arai et al., 2013; Berezin et al., 2001; Zanuttigh & Lamberti, 2007; Zhao et al., 2022). Surge flow is a prominent feature of debris-flow movement at the Jiangjia Ravine (Yunnan Province, China). Debris-flow surges have been found in many places in the world, such as Jiangjia Ravine, Yunnan Province, China (Li et al., 1983), Illgraben, Switzerland (McArdell et al., 2007), Chalk Cliffs, USA (Coe et al., 2010), Rio Moscardo, Italy (Marchi et al., 2002), and Lattenbach Creek, Austria (Huebl & Kaitna, 2021). At Jiangjia Ravine, each debris-flow event has comprised more than a dozen surge flows and several continuous flows (Movie S1). The discharge of surge flows can reach

CHEN ET AL. 1 of 21



Writing – review & editing: Qian Chen, Dongri Song 2,420 m³/s, which is much greater than that of continuous flows; thus, the destructiveness of surge flows is extremely high (Li et al., 1983; Zanuttigh & Lamberti, 2007).

The causes of debris-flow surges are diverse, with many possible explanations. At the watershed scale, the formation of debris-flow surges can be attributed to the blocking effect of landslide dams (Guo et al., 2020) or local terrain fluctuations (Kean et al., 2013). On the other hand, the formation of debris-flow surges is closely related to their inherent properties. Debris-flow surges contain a high fine particle content, which distinguishes them from Newtonian fluids (Chanson et al., 2006; Coussot et al., 2002). The yield stress associated with a jammed network (Coussot & Ovarlez, 2010; Coussot et al., 2005) is believed to be critical for unsteady surges (Bates & Ancey, 2017; Chanson et al., 2006; Wan et al., 1994).

During the propagation of debris-flow surges, particles are deposited on the sides and rear of the flow, after which the deposited material is eroded by subsequent debris-flow surges (Davies, 1986; Li et al., 1983; Zanuttigh & Lamberti, 2007). A surge-flow event composed of multiple surges propagates forward during deposition-erosion (or erosion-deposition) cycles. During erosion-deposition propagation, the eroded deposition layer exhibits relatively a constant amplitude. Similar single surge propagation is obvious in a granular avalanche which generally appear as a single granular surge (Di Cristo et al., 2009; Huang et al., 2022; Razis et al., 2014). Field observation found that the snow avalanche front increases its scale by plowing into an erodible layer of fresh snow, which affects the run-out distance and destructiveness (Sovilla & Bartelt, 2002). As snow avalanches erode material at the front, they deposit snow on the sides and rear of the flow until the snow avalanches starve on the slopes (Bartelt et al., 2007, 2012). Dry granular-flow experiments and depth-averaged numerical simulations with a frictional hysteresis constitutive model (Pouliquen, 1999) can reproduce the surge-like behavior of snow avalanches (Edwards & Gray, 2015; Edwards et al., 2021; Razis et al., 2014). On a slope where dry granular flow begins to flow, the surface is unstable, and a steep particle front develops. The erodible layer is completely carried away, causing the amplitude of the particle front to increase. Moreover, particles are deposited behind and on both sides of the flow to form a stationary erodible layer, which is significantly different from a conventional roll wave and is termed the erosion-deposition surge (Edwards & Gray, 2015; Edwards et al., 2021; Viroulet et al., 2019).

There is a subtle balance in the erosion-deposition propagation for these flow-type mass movements, which determines whether overall growth or decay occurs in the total mass and ultimately affects the destructiveness. The erosion-deposition processes of debris-flow surges have been captured by field observations (Marchi et al., 2002; Zanuttigh & Lamberti, 2007), but specific measurements for confirming these processes are lacking. Correspondingly, when evaluating the destructiveness of surge flows, the total momentum is merely considered the momentum carried by the surge front, and the possible momentum hidden under the surge front is neglected. This conventional approach of momentum considerations may result in a systematic underestimation of mobility and destructiveness. Therefore, tangible evidence for identifying the erosion-deposition propagation of surge flows and a proper approach for quantifying its effect on debris-flow destructiveness are warranted.

There are two approaches for investigating the dynamic process of debris flows. Based on high-tech observational equipment, the local movement information of debris flows can be obtained to infer dynamic processes (Aaron et al., 2023; Berger et al., 2011; McCoy et al., 2012; Nagl et al., 2020). However, due to the destructiveness of debris flows, internal measurements and their accuracy are difficult to guarantee. Alternatively, the dynamic mechanisms of debris flows can be theoretically inferred (Arai et al., 2013; Davies, 1986; Iverson, 2012; Pudasaini & Fischer, 2016). However, the deduced results lack verification with field data, resulting in poor practicality. Due to the complexity of debris-flow movement, neither approach can reveal the real dynamic process of debris flows.

In this study, a combination of field observation and theoretical analysis is used to reveal the erosion patterns and hidden momentum of debris-flow surges. The erosion-deposition propagation is directly confirmed based on the surge-depth hydrographs measured by ultrasonic sensors at the Jiangjia Ravine (Yunnan Province, China). Using simple hydraulic jump equations, the eroded deposition depth of surge flows is quantified and two erosion patterns can be revealed. The total momentum, including both the momentum carried by the surge front and the contribution from the deposition layer eroded by surge flow, is further quantified. The hidden momentum under debris-flow surges is verified via the field observation of surge flows.

CHEN ET AL. 2 of 21



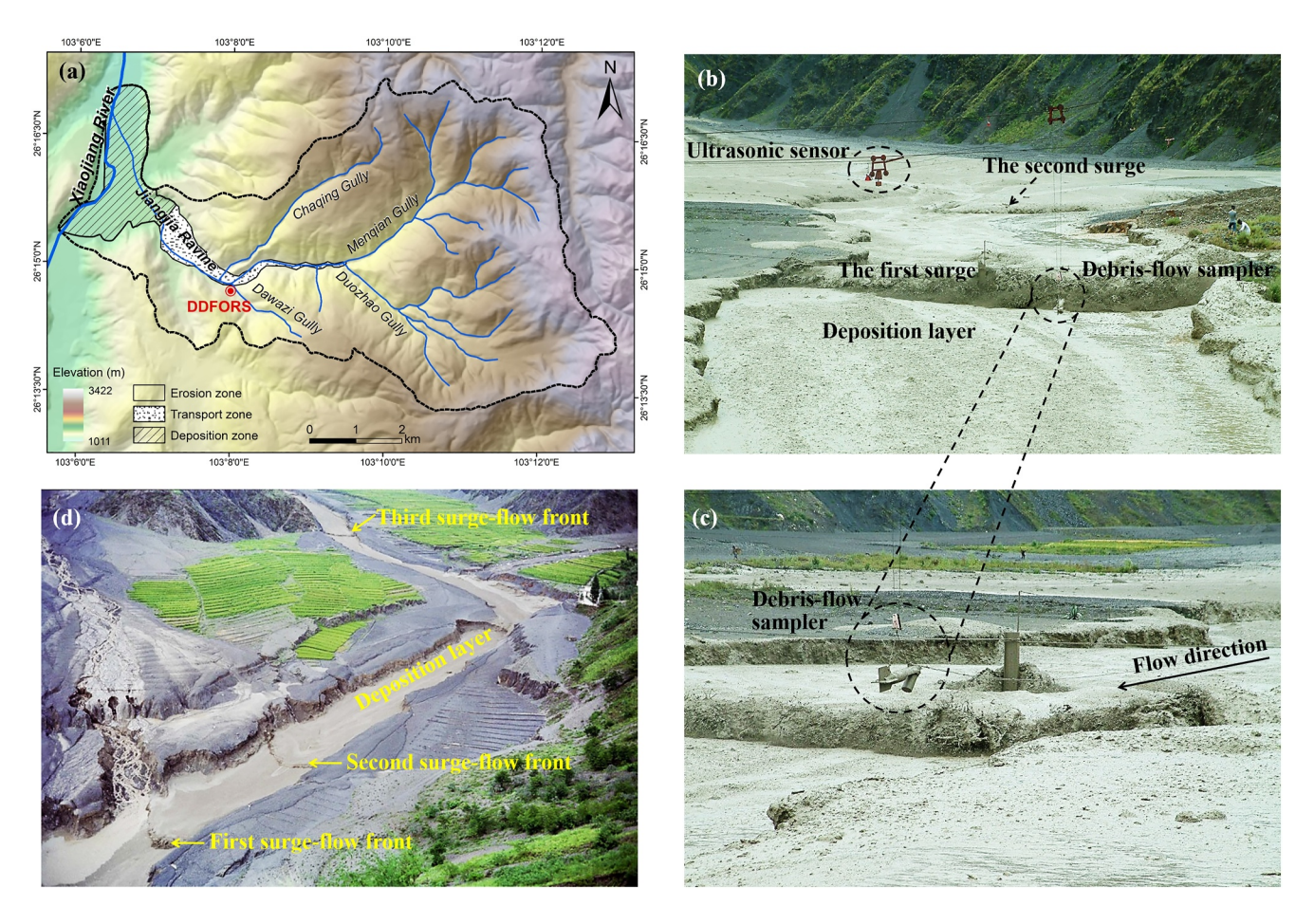


Figure 1. Jiangjia Ravine (Yunnan Province, China). (a) The overview of the Jiangjia Ravine. (b) Field observation of debris flow. (c) Details of debris-flow sampling. (d) Movement of surge flows.

2. Characteristics of Debris Flows at the Jiangjia Ravine

2.1. Debris-Flow Observation at the Jiangjia Ravine

The Jiangjia Ravine is located in Yunnan Province, China, and is famous for its frequent debris flows. The main channel is 13.9 km long with a drainage area of 48.6 km², and it is a tributary of the Xiaojiang River in the upper reaches of the Yangtze River (Figure 1a). In the 1960s, the Institute of Mountain Hazards and Environment, Chinese Academy of Sciences, established the Dongchuan Debris Flow Observation and Research Station (DDFORS) at the Jiangjia Ravine. Long-term observation and research on the initiation, transportation, and accumulation of debris flows have been carried out, and a relatively complete debris-flow database has been established that contains information about more than 400 debris-flow events (Cui et al., 2005; Kang et al., 2004; Wu et al., 1990).

The main debris-flow kinetic parameters measured by DDFORS include the surge-front speed v_s (m/s), surge-front depth h_s (m), and bulk density ρ (kg/m³). The surge-front speed v_s is equal to the length L of a straight channel divided by the time t recorded by stopwatches for a debris-flow surge front to pass through. The surge-front depth h_s refers to the depth of a debris-flow surge front relative to the previous debris-flow deposition, and is measured by an ultrasonic sensor (Figure 1b). At the observation section, the ultrasonic sensor was installed directly 10 m above the channel. The ultrasonic sensor model is Airanger SPL (Siemens Milltronics Process Instruments Inc). The sampling frequency of the ultrasonic sensor is 10 Hz and the measuring range is 0.3–60.0 m. Accuracy is $\pm 0.25\%$ of the range or 6 mm, and resolution is 0.1% of the range or 2 mm, whichever is greater. The measured surge-front depths were the difference between the installation height (10 m) and the measured values of the ultrasonic sensor, and were calibrated based on field manual measurements. Debris-flow material samples

CHEN ET AL. 3 of 21



Table 1Seven Surge-Flow Events Monitored at the Jiangjia Ravine From 1999 to 2001

Event	Surge-front depth h_s , (mean \pm standard deviation, m)	Surge-front speed v_s , (mean \pm standard deviation, m/s)	Bulk density ρ , (mean \pm standard deviation, kg/m ³)	No. of surges	Bed slope θ (°)
1999-7-16	$0.4-2.0$, (0.9 ± 0.4)	$3.6-8.0, (5.6 \pm 1.0)$	$1,740-2,210, (2,056 \pm 190)$	19	3.7
1999-7-24	$0.3-1.8, (0.7 \pm 0.3)$	$5.6-10.0, (7.1 \pm 1.0)$	$1,830-2,290, (2,169 \pm 154)$	51	
2000-7-6	$0.4-1.1$, (0.6 ± 0.2)	$4.8-9.1$, (7.2 ± 1.3)	$1,630-2,290, (2,134 \pm 234)$	20	
2000-8-9	$0.4 - 1.8$, (1.0 ± 0.5)	$5.7-10.3$, (7.7 ± 1.2)	$2,200-2,360, (2,273 \pm 71)$	16	
2000-8-29	$0.4-1.1$, (0.6 ± 0.2)	$4.7-7.9$, (6.0 ± 1.0)	$1,900-2,200, (2,076 \pm 84)$	25	
2001-7-19	$0.3-1.0$, (0.6 ± 0.2)	$5.7-8.7$, (7.3 ± 1.0)	$2,000-2,370, (2,190 \pm 121)$	24	
2001-7-24	$0.4-1.1$, (0.7 ± 0.2)	$5.3-10.4$, (8.0 ± 1.5)	$2,000-2,250, (2,188 \pm 108)$	16	

were collected from the debris-flow surge front (Figure 1b). The sampler was installed in a lead fish. The sampling procedure for the debris-flow sampler is detailed in Figure 1c. Initially, the sampler was placed close to the bed and then raised using hanging cables and a pulley when the debris-flow surge had arrived. The inner diameter of the sampler is 18 cm and the volume is 14 L. The maximum particle size actually collected by the sampler is 10 cm, and its content is also very small. For the particles larger than 0.25 mm, the sieve analysis method was used for particle size distribution analysis. For the particles smaller than 0.25 mm, the pycnometer method was used. The bulk density ρ of debris-flow material sample was estimated using the mass-to-volume ratio. Long-term field observations revealed that surge-flow propagation was the most prominent feature of the Jiangjia Ravine debris flows (Chen et al., 2023; Cui et al., 2005; Kang et al., 2004). Dozens of surge flows are required to drive one debris-flow event downstream to the observation section, and smaller debris flows can only starve in the channel (Davies et al., 1992; Li et al., 1983).

In this study, the field observation of 7 debris-flow events, including 171 surge flows at the Jiangjia Ravine from 1999 to 2001 is used to reveal the destructiveness of surge flows. In Figure 1d, a surge-flow event consists of multiple surge flows, and surge-flow fronts appear as laminar flows with little violent splashing. Each surge flow moving over a deposition layer shows a relatively steep front (Movies S1 and S2). The ranges of surge-front depth, surge-front speed, discharge, bulk density, and number of surge flows for each surge-flow event are summarized in Table 1. For the 171 surge flows, the surge-front depth ranges from 0.3 to 2.0 m, the surge-front speed ranges from 3.6 to 10.4 m/s, and the bulk density ranges from 1,630 to 2,370 kg/m³. Additionally, the means and standard deviations of these measured parameters are provided in Table 1, indicating the scatter of the field observation data. Given the idiosyncrasies of natural settings, there is an inevitable scatter in the field observation data. The scatter of field observation data mainly comes from three aspects. First, in a surge-flow event consisting of multiple surges, these surges vary in scale (Movie S1), which naturally leads to variation in the measured data. Second, the flow surface of a debris-flow surge rises and falls rapidly, resulting in a relatively steep profile, unlike the almost flat surface of tidal bore in water flow (Leng & Chanson, 2017). This relatively steep flow surface may cause the measured data scatter. Third, the ultrasonic sensor sampling frequency is limited (10 Hz), which likely affects the measurement data. Although the interpretation of field observations is often hindered by the inevitable scatter, the essential value of the field observation data is that it is free of the scale effect. Specific information on 171 surge flows, such as the start time, surge-front depth, surge-front speed, and bulk density, is available from Hong (2016).

2.2. Erosion-Deposition Propagation of Surge Flows at the Jiangjia Ravine

The field observation of the Jiangjia Ravine debris flows revealed that in one debris-flow event, initial surge flows adhered to the rough bed along the path, causing the flow to lose material and become thinner (an online movie (Chen & Song, 2024a) is available at https://doi.org/10.12380/Debri.msdc.000020). These surge flows eventually stop on channel bed with the deposition layer (Figure 1d), which is termed "pavement" (Davies et al., 1992; Li et al., 1983). After "pavement", this deposition layer with a certain thickness stays on the bed (Li et al., 1983). After a surge-flow event, there are flood processes, the deposition by the "pavement" of surge flows would be eroded away by waterflow, which makes the channel slope almost constant. Figures 2a–2h shows surge-depth hydrographs of the 7 surge-flow events measured by ultrasonic sensors at the Jiangjia Ravine from 1999 to

CHEN ET AL. 4 of 21

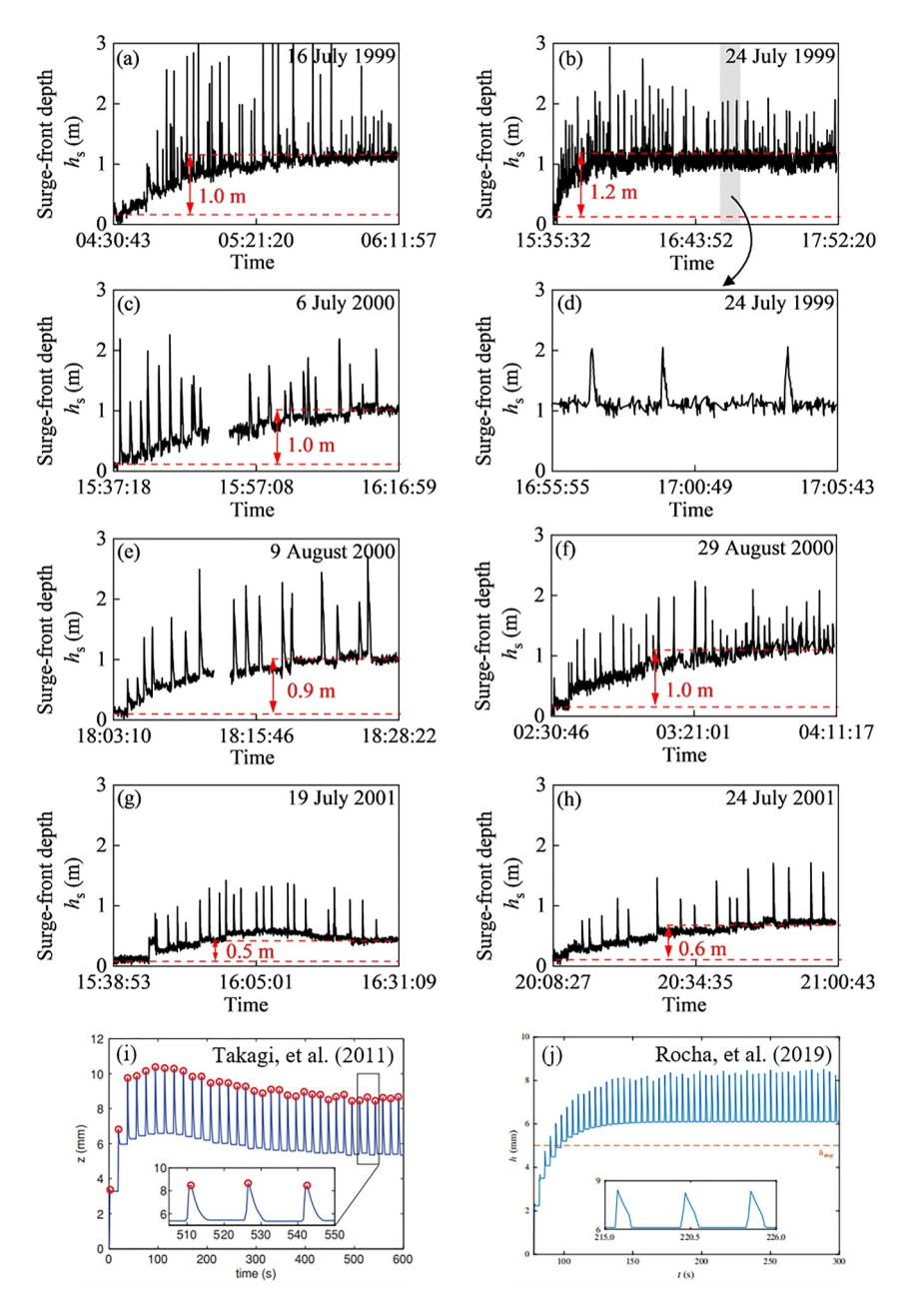


Figure 2. The surge-depth hydrographs of the 7 surge-flow events measured by ultrasonic sensors. Surge flows on (a) 16 July 1999, (b) 24 July 1999, (c) 6 July 2000, (d) a detailed view of the event on 24 July 1999 in panel (b), (e) 9 August 2000, (f) 29 August 2000, (g) 19 July 2001, (h) 24 July 2001. Numbers in red are estimated depths of deposition layers. The datum of each surge-front depth is the channel surface prior to the occurrence of surge flows, and the elevation of this channel surface is set as zero. The surge-depth hydrographs of dry granular flow surges by small-scale experiments in panel (i) (Takagi et al., 2011) and numerical simulations in panel (j) (Rocha et al., 2019).

2001. Figure 2d provides a detailed view of a surge-flow event on 24 July 1999 in Figure 2b, and each debris-flow surge with a steep flow surface is similar to the roll wave in open channel flow. In Figures 2a–2h, each surge-flow event is composed of multiple surge flows, and the surge-flow event is manifested in the measured depth hydrographs as a packet composed of multiple debris-flow surges. In each surge-flow event, a spike represents a surge-front depth measured by ultrasonic sensor when a surge front passes through the observation section. The intervals between surges remain relatively constant, reflecting the obvious periodicity of surge flows. Importantly, there are obvious accumulations at the base level, which directly verifies that surge flows propagate on the erodible layer instead of the rigid bed at the Jiangjia Ravine (Figures 2a–2h). After the movement of one debris-

CHEN ET AL. 5 of 21



flow event consisting of multiple surge flows, the initial base level is elevated and the deposition layer is formed, suggesting that deposition dominates over erosion in the "pavement" process.

The subsequent surge flow entrains the deposition layer formed by the "pavement" to expand its size (Movie S3) and to move further than the previous surge flows until it starves in the channel. Based on physical experiments and field observation at the Jiangjia Ravine, the deposition layer formed by the "pavement" is also movable (Wu et al., 2003b). During the mobilization of the deposition layer by surge flows, surge-flow erosion gradually increases until it balances with erodible deposition, and steady erosion-deposition eventually occurs. In a surgeflow events, the depth of the deposition layer tends to remain relatively constant as the erosion-deposition cycle of debris-flow surges. The height between the two red dashed lines represents the relative constant deposition depth in each event (Figures 2a-2h). Debris-flow surges propagate forward with this steady erosion-deposition, which is similar to the erosion-deposition surges in dry granular flows (Edwards & Gray, 2015; Rocha et al., 2019; Takagi et al., 2011). The surge-depth hydrographs of surge-flow events are not as ideal as those in these smallscale experiments (Figure 2i) and numerical simulations (Figure 2j), mainly because there are inevitable scatters in field observation data in natural settings. The essential value of the field observation data is that it is free of the scale effect, and the scatter of the field observation data does not alter the physical mechanisms. In small-scale experiments (Takagi et al., 2011) and numerical simulations (Edwards & Gray, 2015; Rocha et al., 2019) of dry granular flows, a non-erodible substrate is explicitly set below an erodible layer. However, for debris-flow surges in natural settings, the erodible deposition layer contains erodible pre-event deposition, in addition to the fresh deposition formed by the "pavement" of current surge flows.

Here, we adopt a debris-flow event on 2 August 2023, at the Jiangjia Ravine to illustrate the downward erosion ability of surge flows (an online movie (Chen & Song, 2024b) is available at https://doi.org/10.12380/Debri.msdc.000019). Figure 3 shows the typical moments of erosion-deposition propagation during a surge-flow event and channel-bed evolution at the Jiangjia Ravine. Prior to the surge-flow event, the channel bed was covered by pre-event deposition. There is a muddy stream flow in the channel, which is a precursor to debris-flow outbursts (Figure 3a). A debris-flow surge passes through the observation section in Figures 3b and 3c. After this debris-flow surge, fresh deposition is formed by the "pavement" of surge flow (Figure 3d). A comparison of the channel before and after the surge-flow event (Figures 3a and 3d) reveals that there are obvious mud marks on the channel bank. In Figure 3d, the deposition includes pre-event deposition and fresh deposition. At the end of the event (with 23 surge flows), the debris flows became diluted. As subsequent dilute debris flows and debris floods pass, fresh deposition is carried away, and an eroded step appears in the pre-event deposition (Figure 3e). The depth of this eroded step can reach approximately 1.2 m (Figure 3f). This reveals that a debris-flow surge has significant downward erosion ability. In other words, during debris-flow surge propagation, there is potential downward erosion into pre-event deposition, rather than being limited by the fresh deposition formed by surge-flow "pavement".

Field observation at the Jiangjia Ravine showed that the subsequent surge flow carried away the deposition layer (Figure 3) and formed a larger surge flow to move forward freely at a maximum velocity higher than 10 m/s over a gentle slope less than 5°. This indicates that the deposition layer is conducive to the movement of subsequent surge flows, which may be an important reason for the high-speed movement of surge flows on gentle slopes (Kang et al., 2004; Wu et al., 2003a; Zhang et al., 2003). Research on erosion is notoriously difficult, and estimating eroded deposition depth by various means is the key to revealing the potential destructiveness of debris-flow surges.

3. The Erosion Patterns of Debris-Flow Surges

3.1. Two Possible Erosion Patterns Revealed by Simple Hydraulic Jump Equations

The movement of one debris-flow event composed of multiple surge flows is complicated, but each surge flow follows a self-similar propagation process through erosion and deposition. In the erosion-deposition propagation of a surge flow, the depth and speed of the surge front are easy to measure, and the deposition depth hidden under the debris-flow surge is the key to revealing the erosion and destructiveness of surge flows. Field observation shows that the macroscopic phenomenon of a debris-flow surge is analogous to the propagation of a dam break wave (Capart & Young, 1998; Leal et al., 2006) or a tidal bore (Chanson, 2012; Chanson et al., 2011; Leng & Chanson, 2017) over static water, and the movement of a granular surge (Di Cristo et al., 2009; Razis et al., 2014). The hydraulic jump equations are widely applied to flows beyond water flow, such as dry granular flows

CHEN ET AL. 6 of 21





Figure 3. Typical moments of the surge-flow event and channel-bed evolution at the Jiangjia Ravine. (a) Prior to the surge-flow event; (b and c) an approaching debrisflow surge in motion. The direction of incoming flow is from lower left to upper right (the blue arrows). (d) Deposition in the channel after the debris-flow surge in panels (b and c). (e and f) Formation of an eroded step into the pre-event deposition after the surge-flow event.

(Briukhanov et al., 1967; Eglit et al., 2020; Razis et al., 2014) and viscous-plastic suspensions (Ugarelli & Di Federico, 2007). Consequently, the similarity of macroscopic motion between water flow and flow-type mass movements, and the universal applicability of hydraulic jump equations motivate the application of these equations to debris flow surges. An analysis quite similar to that for dam-break waves (Ancey & Cochard, 2009; Chanson et al., 2006; Leal et al., 2006; Spinewine & Zech, 2007; Zech et al., 2008) and tidal bores (Khezri & Chanson, 2012; Leng & Chanson, 2017; Reungoat et al., 2017) in supercritical flows may be performed to predict the deposition depth under the debris-flow surge.

3.1.1. Simplified Hydraulic Jump Model of Debris-Flow Surges

A surge flow is an unsteady flow for a stationary observer on the bank (Figure 4a). As observed by an observer traveling at surge-front speed, the surge flow can be in a quasi-steady state. In this scenario, the unsteady flow conditions can be solved as a quasi-steady flow situation using the conservation equations of continuity and momentum. This reference frame transformation treatment is often used in hydraulic jumps in open channel flow, and these conservation equations are commonly referred to as hydraulic jump equations (Chanson, 2004). Based on the field observation, the debris flows at the Jiangjia Ravine approach liquefaction (Chen et al., 2023). At a high shear rate, the apparent viscosity of the yield stress fluid is significantly reduced, and the fluid transforms to a

CHEN ET AL. 7 of 21



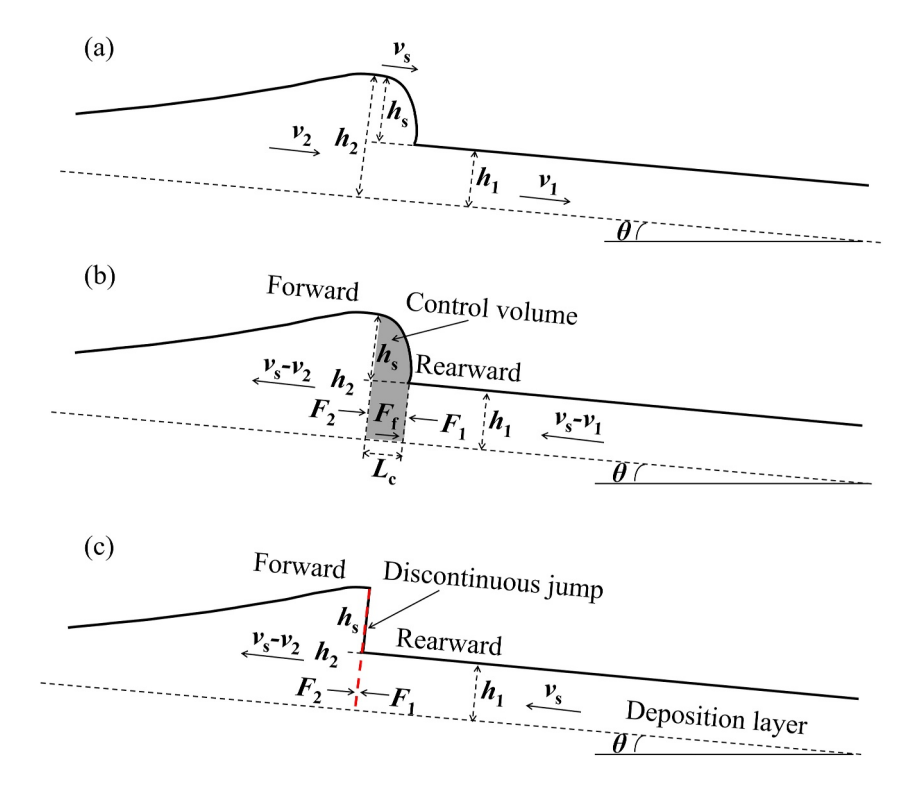


Figure 4. Schematic illustration of surge flow simplified to a positive surge. In the reference frame in panel (a), the observer is stationary. In the reference frame in panels (b) and (c), the observer moves with the surge flow at v_s . The debris-flow surge front is considered as a control volume in panel (b), and the debris-flow surge front is simplified as a discontinuous jump in panel (c).

Newtonian fluid (Coussot, 1995). Field observation at the Jiangjia Ravine indicates that debris-flow surges can move at maximum velocities higher than 10 m/s; thus, it is acceptable not to consider the non-Newtonian rheological behavior of surge flows. Noticeably, the erosion-deposition propagation of surge flow has a relatively constant eroded deposition depth, and the erosion process with mass exchange is not considered. This scenario can be regarded as a fixed-boundary problem with steady erosion. Analogous to dam-break waves or tidal bores in a channel initially filled with water, a steady moving surge flow with a constant deposition layer of depth h_1 (Figure 4) is termed a positive surge in hydraulics (Chanson, 2004).

In a channel with a slope less than 5°, the surge flows spread across the entire channel and the flow cross section exhibits a rectangular shape (Figure 1d). For simplicity, this study focuses on a simplified two-dimensional surge flows in a rectangular channel with a gentle slope (Figure 4). The configuration of three-dimensional surge flows is presented in Text S1 in Supporting Information S1.

In Figure 4a, a surge flow moves downstream with surge-front speed v_s and depth h_s . The velocity and flow depth of forward surge are v_2 and h_2 , respectively. The flow depth and velocity of the deposition layer are h_1 and v_1 , respectively. In the reference frame where the observer and the surge flow move together, the movement of a surge is illustrated in Figure 4b. The surge front is taken as the control volume (the gray shaded area). L_c is the characteristic length of the control volume. ρ_2 and ρ_1 are the bulk densities forward and rearward of the control volume, respectively. F_2 and F_1 are the pressure forces acting forward and rearward, respectively, of the control volume, respectively, $F_1 = 0.5k_1\rho_1gh_1^2\cos\theta$, $F_2 = 0.5k_2\rho_2gh_2^2\cos\theta$. F_f is the flow resistance acting beneath the control volume. In Figure 4b, the terms v_s - v_2 and v_s - v_1 are relative velocities with respect to the movement of the surge front (Chanson, 2012; Stoker, 1957). The continuity and momentum equations are established:

$$\rho_1(v_s - v_1)h_1 = \rho_2(v_s - v_2)h_2 \tag{1}$$

$$\beta_2 h_2 \rho_2 (v_s - v_2)^2 - \beta_1 h_1 \rho_1 (v_s - v_1)^2 = \frac{1}{2} k_1 \rho_1 g h_1^2 \cos \theta - \frac{1}{2} k_2 \rho_2 g h_2^2 \cos \theta - G \sin \theta - F_f$$
 (2)

CHEN ET AL. 8 of 21



where θ is the channel inclination, $\theta = 3.7^{\circ}$ for the Jiangjia Ravine, and g is the acceleration due to gravity (9.81 m/s²). G is the weight of the control volume. β_2 and β_1 are the velocity profile correction coefficients forward and rearward of the control volume, respectively. k_2 and k_1 are the earth pressure coefficients forward and rearward of the control volume, respectively. The k_2 and k_1 are also called pressure correction coefficients in dam break waves and tidal bores (Chanson, 2004). The depth h_2 forward of the surge is equal to the sum of the deposition depth h_1 and surge-front depth h_3 , i.e., $h_2 = h_1 + h_3$.

The following important simplifications and assumptions are considered for revealing the erosion-deposition propagation of debris-flow surges using simple hydraulic jump Equation 1 In Figure 4c, the debris-flow surge is considered a discontinuous jump with zero viscosity. Therefore, the flow resistance F_f and weight G can be neglected. (b) In dam-break waves or tidal bores, there is a significant difference in sediment content between the waves and the bed, which makes the flow density significantly inhomogeneous (Khezri & Chanson, 2012; Leal et al., 2006; Leng & Chanson, 2017; Reungoat et al., 2017). However, as the debris-flow surge moves at high speed and its solid and fluid phases are homogeneously mixed, the density at the debris-flow surge can be regarded as uniform. In the erosion-deposition propagation of debris-flow surges, the deposition is formed by previous well-mixed surge flows, and the density of the underlying deposition can be considered similar to that of the overlying surges. Thus, the density difference between the debris-flow surges and the underlying deposition can be neglected. The bulk density ρ is constant for the debris-flow surge front. (c) It is assumed that the vertical velocity profile is uniform, i.e., the velocity profile correction coefficient $\beta_2 = \beta_1 = 1$ (Faug, 2015). (d) For a liquefied debris flow, it is assumed that the earth pressure coefficient is $k_2 = k_1 = 1$. These depth-averaged mass and momentum conditions are essentially the same as those for hydraulic jumps (Ippen, 1951; Rouse, 1938) and dry granular avalanches (Gray & Cui, 2007), once assumptions about the bulk density, velocity profile correction coefficient, and earth pressure coefficient are made.

A simplified model of the debris-flow surge is shown in Figure 4c. The high solid content makes the surge flows stay and form deposition layer on the channel bed, which is termed "pavement" (Davies et al., 1992; Li et al., 1983). Based on this initial condition of a stationary deposition layer, *i.e.*, $v_1 = 0$, the conservation equations of continuity and momentum forward and rearward the discontinuous jump is established by considering the Rankine-Hugoniot conditions (Gray & Cui, 2007; Razis et al., 2014):

$$\rho v_{s} h_{1} = \rho (v_{s} - v_{2}) h_{2} \tag{3}$$

$$\rho h_2 (v_s - v_2)^2 - \rho h_1 v_s^2 = \frac{1}{2} \rho g h_1^2 \cos \theta - \frac{1}{2} \rho g h_2^2 \cos \theta$$
 (4)

Combined with the boundary condition of flow depth ($h_2 = h_1 + h_s$), the deposition depth h_1 and forward velocity v_2 can be determined. The dimensionless solutions of the deposition depth h_1 are:

$$\left(\frac{h_1}{h_s}\right)_{a} = \frac{1}{2} \left(Fr_s^2 - \left(\frac{1}{4} - 3Fr_s^2 + Fr_s^4\right)^{1/2} - \frac{3}{2} \right)$$
(5a)

$$\left(\frac{h_1}{h_s}\right)_b = \frac{1}{2} \left(Fr_s^2 + \left(\frac{1}{4} - 3Fr_s^2 + Fr_s^4\right)^{1/2} - \frac{3}{2} \right)$$
(5b)

Correspondingly, the dimensionless solutions of the forward velocity v_2 are:

$$\left(\frac{v_2}{v_s}\right)_a = \frac{1}{2} \left(\frac{\left(\frac{1}{4} - 3Fr_s^2 + Fr_s^4\right)^{1/2}}{Fr_s^2} + \frac{1}{2Fr_s^2} + 1\right)$$
(6a)

$$\left(\frac{v_2}{v_s}\right)_a = \frac{1}{2} \left(\frac{-\left(\frac{1}{4} - 3Fr_s^2 + Fr_s^4\right)^{1/2}}{Fr_s^2} + \frac{1}{2Fr_s^2} + 1 \right)$$
 (6b)

CHEN ET AL. 9 of 21



where Fr_s is the surge-front Froude number $(Fr_s = v_s/\sqrt{gh_s\cos\theta})$. Equations 5 and 6 are analogous to the theoretical development of Stoker (1957). The theoretical solutions for the deposition depth h_1 (Equations 5a and 5b) and forward velocity v_2 (Equations 6a and 6b) are both positive values, and $(h_1/h_s)_a < (h_1/h_s)_b$ and $(v_2/v_s)_a > (v_2/v_s)_b$. In addition, these theoretical solutions satisfy the conditions for generating a positive surge (Figure 4c): (a) the rearward Froude number $Fr_1 > 1$ ($Fr_1 = v_s/\sqrt{gh_1\cos\theta}$); (b) the forward Froude number $Fr_2 < 1$ ($Fr_2 = (v_s - v_2)/\sqrt{gh_2\cos\theta}$); and (c) the surge-front speed $v_s > v_2 > v_1$. Details of the verifications are presented in Text S2 in Supporting Information S1. Therefore, both solutions are theoretically plausible.

According to the measured surge-front speeds and surge-front depths of the 108 steady surge flows from 7 surge-flow events at the Jiangjia Ravine, using Equation 5a, the calculated deposition depths are 0.08–0.67 m, 0.01–2.6 m, 0.02–0.11 m, 0.02–0.23 m, 0.03–0.08 m, 0.02–0.08 m, and 0.02–0.07 m, respectively. Using Equation 5b, the calculated deposition depths of these 7 surge-flow events are 0.58–3.11 m, 2.69–7.29 m, 2.14–5.43 m, 3.34–7.98 m, 1.56–4.25 m, 2.99–6.36 m, and 2.72–9.25 m, respectively. Due to the lack of direct measurements of the deposition depth, the correctness of the calculated deposition depths is difficult to verify. Furthermore, the calculated deposition depths of each surge-flow event are quite scattered. Nevertheless, the surge-depth hydrographs demonstrate that the deposition depth formed by the "pavement" is relatively constant (Figures 2a–2g). Therefore, the significance of Equation 5 is not that it can calculate the specific deposition depth of a single surge. Rather, it can be used to quantitatively divide the erosion pattern of surge flows. The depth of the deposition layer represents the potential erosion ability of surge flows. Equation 5 indicates that for a surge flow, there are two possible erosion depths. In other words, there are two erosion patterns in the erosion-deposition propagation of surge flows.

3.1.2. Division of the Erosion Patterns of Debris-Flow Surges

Considering the deposition depth h_1 as the eroded depth, the erosion pattern of surge flow can be quantitatively divided. Based on the relationship of the two theoretical solutions of dimensionless eroded deposition depth $(h_1/h_s)_a < (h_1/h_s)_b$ (Equation 5), for surge flows with the same flow discharge, two erosion patterns may exist. (a) Shallow erosion: the surge flow moves over a shallow deposition layer, and maintains a large depth at the front (Figure 5a). Such surge flows exhibit a steep front relative to the shallow deposition layer in the channel. For this shallow erosion pattern, the small solution for the eroded deposition depth (Equation 5a) may be the eroded depth. (b) Deep erosion: the surge flow moves over a deep deposition layer. Such surge flows exhibit a shallow front relative to the deep deposition layer in the channel (Figure 5b). For this deep erosion pattern, the large solution of the eroded deposition depth (Equation 5b) may be the eroded depth.

Based on the relationships between the dimensionless eroded deposition depth and surge-front Froude number (Equations 5a and 5b), a surge flow with a constant surge-front Froude number (equivalent to constant flow discharge) may have two eroded depths. With the dimensionless eroded deposition depth $h_1/h_s = 0.71$ as the inflection point, one eroded depth is shallow (blue curve in Figure 6a), and the other is deep (red curve in Figure 6a), corresponding to the shallow and deep erosion patterns described in Figure 5, respectively. In Figure 6a, the dimensionless eroded deposition depth h_1/h_s shows an opposite trend with increasing surge-front Froude number Fr_s . For shallow erosion (blue curve in Figure 6a), as the surge-front Froude number Fr_s increases, the dimensionless eroded deposition depth h_1/h_s slowly decreases from 0.71 to 0.0. Conversely, for deep erosion (red curve in Figure 6a), as the surge-front Froude number Fr_s increases, the dimensionless eroded deposition depth h_1/h_s significantly increases from 0.71.

These two erosion patterns quantified by the relationship between the dimensionless eroded deposition depth h_1/h_s and surge-front Froude number Fr_s (Equations 5a and 5b) can be synthesized by the relationship between the dimensionless eroded deposition depth h_1/h_s and rearward Froude number Fr_1 (Equation 7). Based on the continuity and momentum equations (Equations 3 and 4), the relationship between the dimensionless eroded deposition depth h_1/h_s and the rearward Froude number Fr_1 can be established:

$$\frac{h_1}{h_s} = \frac{2}{\sqrt{1 + 8Fr_1^2 - 3}}\tag{7}$$

CHEN ET AL. 10 of 21

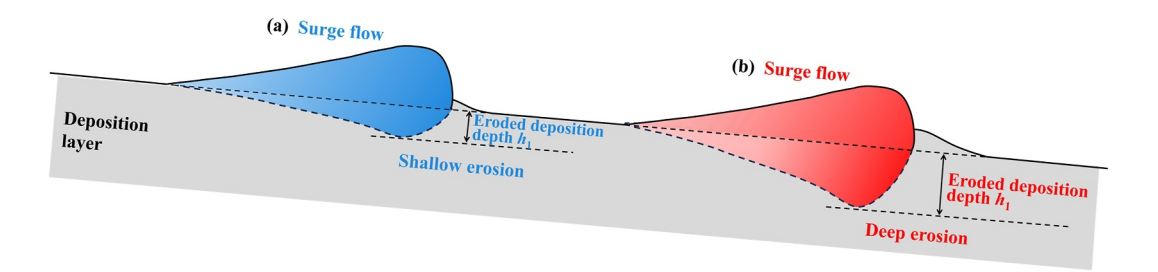


Figure 5. The diagram of surge-flow erosion patterns. (a) Shallow erosion: the eroded deposition depth is shallow and limited. (b) Deep erosion: the eroded deposition depth is deep and unrestricted.

In Equation 7, the rearward Froude number Fr_1 ($Fr_1 = v_s/\sqrt{gh_1\cos\theta}$) represents the dynamics of the surge front and deposition layer. Substituting the two solutions of the dimensionless eroded deposition depth h_1/h_s (Equations 5a and 5b) into Equation 7, the relationship between the rearward Froude number Fr_1 and surge-front Froude number Fr_3 can be expressed as follows:

$$Fr_1^2 = \left(\frac{1}{2} \mp \frac{1}{2} \left(\frac{1}{4Fr_s^4} - \frac{3}{Fr_s^2} + 1\right)^{1/2} - \frac{3}{4Fr_s^2}\right)^{-1}$$
 (8)

In Figure 6b, the dimensionless eroded deposition depth h_1/h_s shows a decreasing trend with increasing rearward Froude number Fr_1 . The dimensionless eroded deposition depth $h_1/h_s = 0.71$ also serves as an inflection point that divides the two erosion patterns. In Figure 6b, the red and blue branches of the theoretical curve of Equation 7 represent deep and shallow erosion, respectively.

3.2. Determination of the Eroded Deposition Depth Under the Surge Front

Determination the eroded deposition depth h_1 is the key to verifying the erosion patterns and quantifying the destructiveness of surge-flow erosion. There are two feasible approaches for determining the eroded deposition depth h_1 .

3.2.1. Eroded Deposition Depth Estimated by Surge-Depth Hydrographs

First, the erosion depth of the surge flow can be approximated by the deposition depth formed by the "pavement", which can be directly estimated from the surge-depth hydrographs (Figures 2a–2g). From the initial moment of each surge-flow event to the steady stage, the eroded deposition depths in 7 surge-flow events at the Jiangjia Ravine range from 0.5 to 1.2 m (Figures 2a–2g). In this approach, eroded deposition depths are

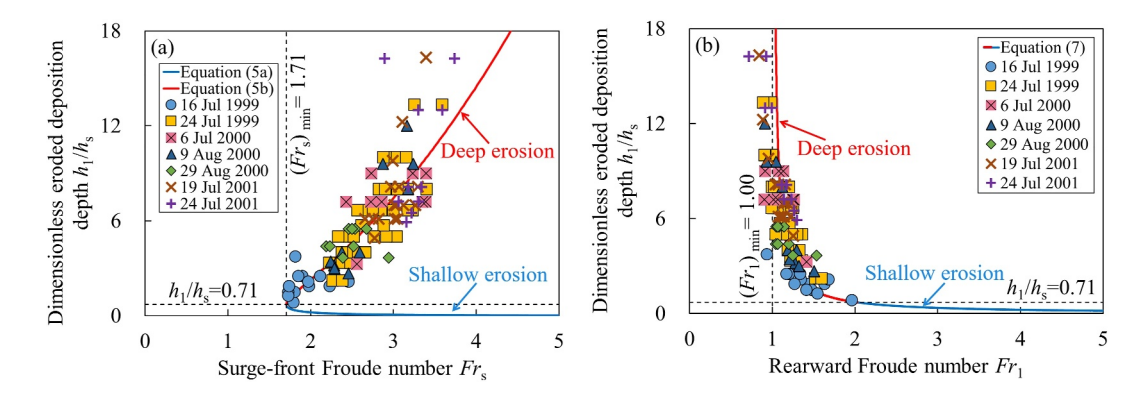


Figure 6. Two erosion patterns of debris-flow surges quantified by the relationship between dimensionless eroded deposition depth h_1/h_s and (a) surge-front Froude number Fr_s , and (b) rearward Froude number Fr_1 . The dashed black lines with $h_1/h_s = 0.71$ delimit the deep and shallow erosions. The dimensionless eroded deposition depths of 108 steady surge flows at the Jiangjia Ravine are calculated from the deposition depth h_1 fitted by Equation 11 and illustrated in Figure 7.

CHEN ET AL.



deduced from the initial elevation (datum) before surge-flow events and do not include possible downward erosion into the pre-event deposition by surge flows. In fact, field observation indicates that there is an eroded step into the pre-event deposition after a surge-flow event (Figure 3). The erosion into the pre-event deposition on the channel bed cannot be determined, so these eroded deposition depths cannot represent the entirely constant eroded depth.

3.2.2. Eroded Deposition Depth Estimated by Hydraulic Jump Equations

The theoretical relationship between the surge-front speed and depth can be used to determine the entirely constant eroded deposition depth h_1 . According to the continuity and momentum Equations 3 and 4, a quadratic equation for the surge-front speed v_s can be obtained:

$$h_1 v_s^2 - 2h_1 v_1 v_s + h_1 v_1^2 - \frac{1}{2}g \cos \theta (2h_1 + h_s) (h_1 + h_s) = 0$$
(9)

There are two solutions for the surge-front speed v_s :

$$v_{s} = \pm \sqrt{\frac{\frac{1}{2}g\cos\theta(2h_{1} + h_{s})(h_{1} + h_{s})}{h_{1}}}$$
 (10)

Since $v_s > v_2$ for a positive surge, only the positive solution is admissible. The theoretical relationship between the surge-front speed v_s and depth h_s is:

$$v_{\rm s} = \sqrt{\frac{\frac{1}{2}g\cos\theta(2h_1 + h_{\rm s})(h_1 + h_{\rm s})}{h_1}}$$
 (11)

Equation 11 indicates that the surge-front speed v_s is related not only to the surge-front depth h_s , but also to the eroded deposition depth h_1 . Equation 11 can be decomposed into Equations 5a and 5b. Accordingly, if the surge-front speed v_s and depth h_s are known, the eroded deposition depth h_1 can be determined by Equation 11. Rather than substituting the surge-front speed and depth of a single surge into Equation 11 to calculate the eroded deposition depth of the surge flow, the eroded deposition depth of each surge-flow event consisting of multiple surges is fitted by Equation 11 using the surge-front speeds and depths of multiple surges in each surge-flow event (Figure 7).

Figures 7a-7g shows the relationship between the surge-front speed v_s and depth h_s for these 7 surge-flow events. These surge-front speeds and depths measured from steady sections on the surge-depth hydrographs are adopted. Based on Equation 11, the eroded deposition depths of these 7 surge-flow events are fitted by the least squares method, and range from 1.5 to 6.5 m, which are greater than the eroded deposition depths estimated by surge-depth hydrographs in Section 3.2.1. This indicates that the deposition layer (Figures 2a-2g) formed by the "pavement" cannot completely represent the total constant eroded depth. In Figures 7a-7g, obviously, these eroded deposition depths fitted by the theoretical relationship between the surge-front speed and depth (Equation 11) should incorporate the eroded pre-event deposition depths, as well as the deposition depths resulting from the "pavement". This echoes the eroded step scoured by the debris-flow surges into the pre-event deposition, as shown in Figure 3f. This further indicates that in the erosion-deposition propagation of surge flows, the balance between erosion and deposition can be disrupted once surge flows have sufficient downward erosion potential and when the eroded deposition layer is unrestricted.

3.3. Erosion-Pattern Verification by Debris-Flow Surges at the Jiangjia Ravine

Using the fitted eroded deposition depths in Figures 7a-7g, the erosion patterns of surge flows are verified. The data points in Figures 6a and 6b show the relationships between the dimensionless eroded deposition depth h_1/h_s and the surge-front Froude number Fr_s and rearward Froude number Fr_1 of the 7 surge-flow events at the Jiangjia Ravine, respectively. These data points fall in the branches with greater dimensionless eroded deposition depths, and the erosion pattern of the surge flows at the Jiangjia Ravine reflects deep erosion. The relationships between

CHEN ET AL. 12 of 21

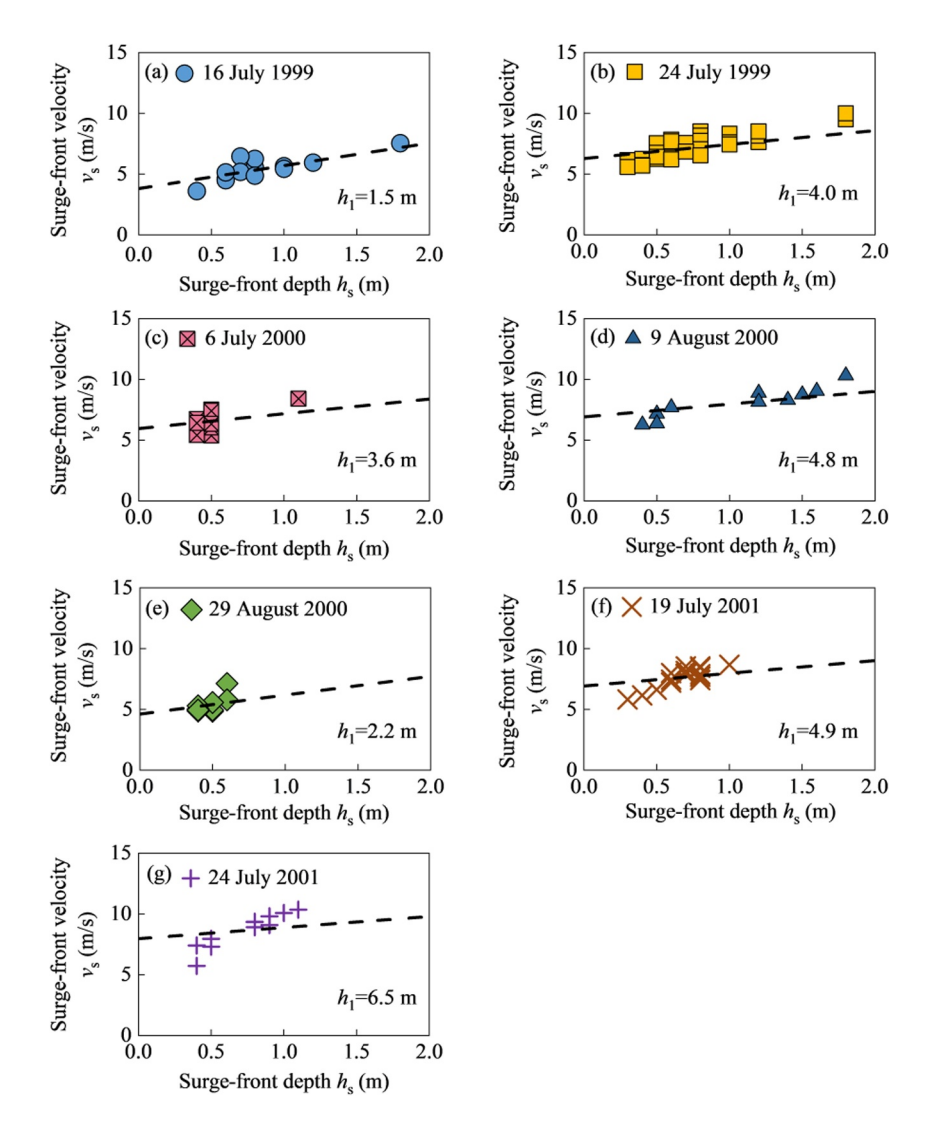


Figure 7. The relationship between surge-front speed v_s and surge-front depth h_s of the 7 surge-flow events. Surge flows on (a) 16 July 1999, (b) 24 July 1999, (c) 6 July 2000, (d) 9 August 2000, (e) 29 August 2000, (f) 19 July 2001, and (g) 24 July 2001. The eroded deposition depth h_1 is fitted by Equation 11 based on the measured constant surge-front speeds and surge-front depths.

the conjugate depth ratio h_2/h_1 and two Froude numbers (the surge-front Froude number Fr_s and rearward Froude number Fr_1) are further used to verify the erosion patterns of surge flow in Text S3 in Supporting Information S1. Based on the fitted eroded deposition depths in Figures 7a–7g, the conjugate depth ratios h_2/h_1 of surge flows at the Jiangjia Ravine are calculated and fall in the deep erosion pattern (the data points in Figure S2 in Supporting Information S1).

Based on the above verification results, the erosion pattern of debris-flow surges at the Jiangjia Ravine is classified as deep erosion. This indicates that surge-front erosion is not limited to the deposition layer formed by "pavement" in surge flows with the deposition-erosion process. If the underlying substrate is not a rigid bed but an erodible pre-event deposition, the surge front would continue to erode downward. The above verification quantitatively reveals the downward erosion observed in Figure 3. Obviously, for this type of surge flow, the momentum carried by the apparent surge front cannot fully represent the destructiveness due to the deep erosion hidden under the surge front. Accordingly, there may be an underestimation in the conventional approach using apparent surge-front momentum to assess the destructiveness of surge flow.

CHEN ET AL. 13 of 21



4. Quantification of Surge-Flow Destructiveness

4.1. Momentum Hidden Under the Surge Front

Based on the erosion-deposition characteristics of surge flows at the Jiangjia Ravine, the total momentum carried by surge flows is significantly higher than that of the apparent surge front. The momentum flux is a direct indicator of the destructiveness of debris flows (Ng et al., 2023; Song et al., 2021, 2023). The momentum flux per unit width is taken, and the total momentum flux of a surge flow can be divided into two main components. One is the momentum carried by the surge front, and its momentum flux is $\rho v_2^2 h_s$. The other includes the momentum hidden under the eroded deposition layer. The mobilized deposition layer at depth h_1 has a velocity v_2 , and the momentum flux hidden under the eroded deposition layer is $\rho v_2^2 h_1$. The total momentum flux of surge flow is the sum of the apparent surge-front flux and the flux hidden under the eroded deposition layer, i.e., $\rho v_2^2 h_s + \rho v_2^2 h_1$.

The momentum ratio *R* can be expressed as the ratio of the total momentum flux of surge flow to that of the surge front:

$$R = \frac{\rho v_2^2 h_s + \rho v_2^2 h_1}{\rho v_2^2 h_s}$$

$$= 1 + \frac{h_1}{h_s}$$
(12)

Based on the relationships between the dimensionless eroded deposition depth h_1/h_s and surge-front Froude number Fr_s (Equation 5) and rearward Froude number Fr_1 (Equation 7), the relationships between the momentum ratio R and surge-front Froude number Fr_s and rearward Froude number Fr_s can be obtained:

$$R_{\rm a} = \frac{1}{2} \left(Fr_{\rm s}^2 - \left(\frac{1}{4} - 3Fr_{\rm s}^2 + Fr_{\rm s}^4 \right)^{1/2} + \frac{1}{2} \right)$$
 (13a)

$$R_{\rm b} = \frac{1}{2} \left(Fr_{\rm s}^2 + \left(\frac{1}{4} - 3Fr_{\rm s}^2 + Fr_{\rm s}^4 \right)^{1/2} + \frac{1}{2} \right)$$
 (13b)

$$R = 1 + \frac{2}{\sqrt{1 + 8Fr_1^2 - 3}} \tag{14}$$

Based on the relationship between the rearward Froude number Fr_1 and surge-front Froude number Fr_s (Equation 8), Equation 14 is equivalent to Equation 13. These theoretical relationships indicate that the total momentum of surge flow not only relies on the surge-front depth h_s and speed v_s (characterized by the surge-front Froude number Fr_s), but is also controlled by the eroded deposition depth h_1 (explicitly included in the rearward Froude number Fr_1).

Figure 8a shows the theoretical relationship between the momentum ratio R and the surge-front Froude number Fr_s . The blue and red curves in Figure 8a represent Equations 13a and 13b, respectively. Notably, the theoretical curve features an inflection point at $(Fr_s)_{\min} = 1.71$, indicating that the relationship between the momentum ratio R and the surge-front Froude number Fr_s is non-monotonic. For the blue curve, as the surge-front Froude number Fr_s increases, the momentum ratio R decreases from 1.71 to unity. Conversely, for the red curve, the momentum ratio R reaches a minimum value of 1.71 and then escalates rapidly with increasing Fr_s . The blue and red curves in Figure 8a correspond to shallow and deep erosion, respectively, with the magnitude of the momentum ratio being intimately linked to the erosion patterns as demarcated by the eroded deposition depth. For the blue curve (Equation 13a), the low momentum ratio suggests that the momentum hidden in the eroded deposition layer is constrained. Consequently, the debris-flow surge is compelled to maintain a steep front, leading to shallow erosion with limited eroded deposition. In contrast, for the red curve (Equation 13b), the high momentum ratio implies substantial momentum beneath the eroded deposition layer. This allows the debris-flow surge to disperse downward, resulting in deep erosion with significant eroded deposition.

Figure 8b shows the theoretical relationship between the momentum ratio R and the rearward Froude number Fr_1 . This theoretical relationship is characterized by its monotonic nature. As the rearward Froude number Fr_1

CHEN ET AL. 14 of 21

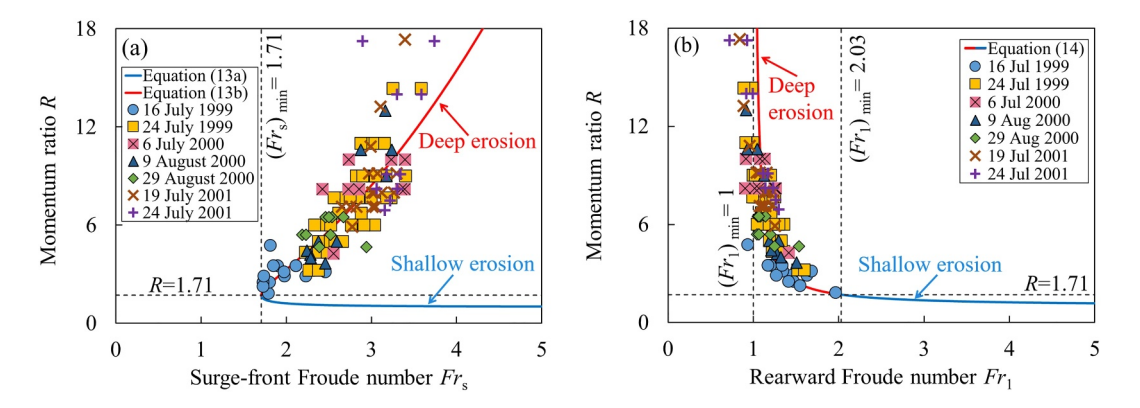


Figure 8. The relationship between momentum ratio R and (a) surge-front Froude number Fr_s , and (b) rearward Froude number Fr_1 . The red and blue curves represent deep and shallow erosion, respectively, which is consistent with Figure 6. The dashed black lines with R = 1.71 delimit the deep and shallow erosions. These data points represent the momentum ratios of 108 steady surge flows at the Jiangjia Ravine, which are calculated from eroded deposition depth h_1 fitted by Equation 11 and illustrated in Figure 7.

increases, the momentum ratio R decreases rapidly from infinity to 1.71. It is noteworthy that, within this theoretical framework, the momentum ratio may not possess an upper limit. In practical scenarios, such elevated momentum could arise from the flip-through impact associated with waves exhibiting steep fronts (Peregrine, 2003). This phenomenon is observed in the impact of water waves on walls (Hofland et al., 2011; Lugni et al., 2006), the impact of a liquefied debris-flow surge on a rigid obstacle (Song et al., 2021), and the advancement of a granular surge across flat terrain (Méjean et al., 2020).

In Figure 8b, the blue and red branches of the theoretical curve represented by Equation 14 correspond to shallow and deep erosion, respectively, as depicted in Figure 8a. The variation in the momentum ratio R with the rearward Froude number Fr_1 is actually controlled by the competition between the eroded deposition depth h_1 and surgefront depth h_s in the two erosion patterns. In the deep erosion, the eroded deposition depth h_1 dominates the surgefront depth h_s . As the rearward Froude number Fr_1 increases from unity to 2.03, the momentum ratio R demonstrates a downward trend (the red branch in Figure 8b). This indicates that the momentum hidden within deep erosion is substantial and decreases as the eroded deposition depth h_1 diminishes (corresponding to an increase in Fr_1). However, due to the considerable depth of the deposition layer, the eroded deposition depth remains significantly greater than the shallow surge-front depth, establishing a lower limit for the momentum ratio at R = 1.71 in the red branch in Figure 8b. This signifies that the total momentum carried by a surge flow is at least 1.71 times the apparent surge front in deep erosion.

In the shallow erosion, the surge-front depth $h_{\rm s}$ dominates the eroded deposition depth $h_{\rm 1}$. This results in a maximum momentum ratio of R=1.71 when the deposition layer is mobilized, but the momentum ratio converges to unity, as the deposition layer becomes fully eroded and incorporated into the surge front, as shown by the blue branch in Figure 8b. Consequently, the total momentum carried by a surge flow can be up to 1.71 times the apparent surge front, even in scenarios of shallow erosion with limited deposition depth. The momentum ratio in deep erosion consistently exceeds that in shallow erosion. Therefore, the momentum hidden in the deposition layer is a non-negligible component, and the destructiveness of surge flow is provided by the momentum hidden in the deposition layer and the momentum carried by the apparent surge front. The momentum associated with the apparent surge front alone cannot be considered a sufficient proxy for the overall destructiveness of the surge flow.

4.2. Destructiveness of Surge Flows at the Jiangjia Ravine

Based on the eroded deposition depth fitted by Equation 11, the field observations of surge flows at the Jiangjia Ravine are employed to verify the theoretical relationships between the momentum ratio R and surge-front Froude number Fr_s (Equation 13) as well as the rearward Froude number Fr_1 (Equation 14). Although the velocity distribution in the vertical profile of a debris flow can differ, potentially causing inaccuracies in the eroded deposition depth fitted by Equation 11. Nevertheless, since momentum conservation is independent of the vertical velocity distribution, this does not compromise the accuracy of the debris-flow momentum.

CHEN ET AL. 15 of 21



In Figures 8a and 8b, the momentum ratios of the 108 surge flows at the Jiangjia Ravine are aligned with the red theoretical curve of Equation 13b and the red branch of the theoretical curve of Equation 14, respectively. This distribution agrees with the theoretical relationships of the momentum ratio. This finding illustrates that the theoretical relationships between the momentum ratio R and surge-front Froude number Fr_s (Equation 13b) and rearward Froude number Fr_1 (Equation 14) are effective in predicting the momentum hidden under the surge front in the erosion-deposition propagation of surge flows.

These data points indicates that the momentum ratios of surge flows at Jiangjia Ravine are greater 1.71 (Figures 8a and 8b). These elevated momentum ratios directly reveal that the eroded deposition layer is a non-negligible source of debris-flow surge destructiveness. Moreover, this finding underscores the importance of considering the destructiveness of surge flows on gentle slopes (the slope at Jiangjia Ravine is less than 5°), thereby challenging the traditional consensus in debris-flow hazard assessment, which typically focuses on the destructiveness of debris flows on steep slopes. Additionally, the distribution of momentum ratios along the deep erosion pattern at Jiangjia Ravine highlights the close relationship between surge-flow destructiveness and erosion patterns during erosion-deposition propagation. Besides the dynamic parameters of the surge front, the eroded deposition depth emerges as a crucial parameter in determining the destructiveness of surge flows during erosion-deposition propagation. Therefore, further research on debris-flow erosion on gentle slopes should focus on the investigation of erosion into substrate deposition.

5. Discussion

5.1. The Limitations in the Theoretical Approach

In the momentum conservation equation (Equation 4), assumptions regarding bulk density, earth pressure coefficients, and velocity profile correction coefficients are employed. In the two-phase debris flow, the ratio of bulk densities rearward and forward the surge may not be unity. Furthermore, the solid particles might be in different active and passive states rearward and forward the surge, resulting in earth pressure coefficients k_2 and k_1 are likely different from unity. These potential deviations from uniform bulk density and isotropic pressure distribution are not considered. These assumptions that the bulk densities are considered constant and earth pressure coefficients k_2 and k_1 are taken as unity hold because the surge flow is fully liquefied, the solid-liquid phases are well-mixed, and the debris-flow surge exhibits quasi-steady state in the traveling reference frame. The velocity profile correction coefficients β_2 and β_1 are taken to be equal to unity, which corresponds to the exact value for plug flows. However, given the varying shapes of velocity profiles, β_2 and β_1 can be taken to be equal to 4/3 for linear velocity profiles, and 5/4 for Bagnold velocity profiles (Faug, 2015; Mejean et al., 2017). As a result, the eroded deposition depth fitted by Equation 11 may be inaccurate. Nevertheless, since momentum conservation does not depend on the vertical velocity profile, this does not affect the accuracy of potential maximum momentum hidden in surge-flow erosion. Therefore, based on these assumptions, the estimates of upper limits on the erosion ability and destructiveness can be obtained using the approximate theoretical approach.

Long-term field observations have demonstrated that erosion-deposition propagation is a significant characteristic of surge flows at the Jiangjia Ravine. Objectively, due to limitations in field observations of debris flows, measurements have been confined to the flow depth and speed of the surge front, leaving out the critical parameter of deposition layer depth. This omission makes it challenging to quantitatively reveal the internal erosion of surge flows and their associated total momentum. To address this, this study proposes an approximate theoretical approach to quantify the erosion and destructiveness of surge flows in the absence of comprehensive field observation data. This approach emphasizes the scientific insights gained from long-term observations of debris flows. The assumptions underlying this theoretical approach do not alter the insights obtained from the long-term observations of debris flows. The alignment between the observations and the model predictions suggests that the fundamental physical elements of this simplified model control the debris-flow surges.

5.2. Why Does a Deep-Erosion Pattern Occur?

With the development of erosion-deposition, the eroded deposition depths tend to reach constant amplitudes (Figure 2). This process is similar to erosion-deposition surges in dry granular flows (Edwards & Gray, 2015; Rocha et al., 2019; Takagi et al., 2011). Based on simple hydraulic jump equations, two erosion patterns of surge flows are revealed by the relationships between the dimensionless eroded deposition depth h_1/h_8 and two Froude

CHEN ET AL. 16 of 21



numbers (the surge-front Froude number Fr_s and rearward Froude number Fr_1), namely, shallow and deep erosion patterns.

The erosion patterns can be further verified through the eroded deposition depth. The constant eroded deposition depth cannot be directly measured. Alternatively, based on the theoretical relationship between surge-front speed and surge-front depth, the eroded deposition depth can be fitted with the measured surge-front speeds and depths of surge flows (Figure 7). The 108 steady surge flows at the Jiangjia Ravine confirm that the surge-flow erosion belongs to the deep erosion (Figure 6). This quantitatively indicates that surge-flow erosion not only occurs in the deposition layer formed by the "pavement" of surge flows, but also scours into the underlying pre-event deposition.

There are two perspectives that explain the deep-erosion pattern of surge flow with deposition-erosion propagation. On the one hand, debris-flow surges have a significant downward erosion ability that is not limited to the shallow deposition formed by the "pavement" of surge flows. This has been confirmed by the surge-flow event on 2 August 2023 at the Jiangjia Ravine (an online movie (Chen & Song, 2024b) is available at https://doi.org/10.12380/Debri.msdc.000019). The eroded step spans the deposition formed by surge-flow "pavement" and preevent deposition (Figure 3f).

On the other hand, the most probable state of a natural phenomenon is the one for which the entropy is maximized or the entropy production rate is minimized (Molnár & Ramírez, 1998; Nanson & Huang, 2008, 2018; Tranmer et al., 2020; Yalin & Ferreira Da Silva, 1999). From the energy perspective, due to the shear at the channel bed and internal flow resistance, the kinetic energy in open channel flow is converted into heat. A hydraulic jump is an important form of energy dissipation (Chanson, 2004). The surge flow is similar to the hydraulic jump in an open channel, and has a remarkable energy dissipation performance. Note that natural processes always follow the pattern with the maximum rate of energy dissipation (Khanfouf et al., 2022; Slepyan, 1993; Ulu et al., 2023). Obviously, deep erosion is more conducive to energy dissipation.

Additionally, deep erosion provides sufficient momentum transfer space for overlying surge flow. A moving surge flow over an unrestricted erodible bed does not stay on the bed surface but rather transmits excess momentum through downward erosion to achieve steady propagation. The overlying surge flow mobilizes the eroded deposition layer, increasing the flow depth of the moving surge flow, which results in momentum being transferred downward into the deposition layer (Song et al., 2022). Thus, during the deep erosion, efficient mixing between debris-flow surges and eroded deposition induces a faster energy dissipation rate and momentum transfer than does the shallow erosion. For the steady propagation of surge flow over an erodible bed, shallow erosion is theoretically plausible, but physically inadmissible. On gentle slopes, a large flowing portion exists beneath a debris-flow surge, and what we see from the flow surface is merely "the tip of the iceberg."

6. Conclusions

Debris-flow surges are destructive. However, few suitable approaches can directly reveal their destructiveness. As a result, the momentum of the surge front is conventionally used as a proxy for surge-flow destructiveness. Instead of relying on high-resolution equipment to obtain information on the surface of debris flows and infer the whole dynamic process of debris flows (Aaron et al., 2023; Kean et al., 2015; McCoy et al., 2012), this study looks into the inside of surge flows based on simple hydraulic jump equations and the field observation of surge flows. The erosion pattern and momentum hidden under debris-flow surges are revealed. The main contribution of this study is to provide a theoretical approach for quantifying the eroded deposition depth and the total momentum carried by debris-flow surges. This approach is conducive to improving the reliability of risk assessment and mitigation for debris-flow surges. The key conclusions are as follows.

- 1. The erosion-deposition propagation of debris-flow surges is confirmed based on surge-depth hydrographs measured by ultrasonic sensors at the Jiangjia Ravine. In the erosion-deposition propagation of surge flow, for the "pavement" of initial surge flows, deposition dominates over erosion, resulting in a growing deposition layer on the channel. As the deposition layer is eroded by subsequent surge flows, surge-flow erosion could reach a balance between erosion and deposition for surge flows.
- 2. In natural settings, the deposition formed by the "pavement" of surge flows is underlain by erodible pre-event deposition instead of a rigid, non-erodible substrate. Debris-flow surges have a significant downward erosion into pre-event deposition rather than being limited by the fresh deposition formed by surge-flow "pavement."

CHEN ET AL. 17 of 21



- 3. Based on simple hydraulic jump equations, the erosion pattern of surge flow can be divided into shallow and deep erosion. Based on the theoretical relationship between surge-front speed and depth, the eroded deposition depth can be fitted with the measured surge-front speed and depth of surge flows. According to the validation of surge-flow field observation, the erosion pattern of debris-flow surges at the Jiangjia Ravine is classified as the deep erosion, which quantitatively indicates the downward erosion ability of debris-flow surges. In deep erosion, the efficient mixing between debris-flow surges and eroded deposition induces a higher energy dissipation rate than that in shallow erosion. The deep eroded deposition layer provides sufficient space for momentum transfer from the overlying surge flow.
- 4. The destructiveness of surge flow is inextricably linked to the surge-flow erosion pattern. The momentum ratio is characterized by two Froude numbers (the surge-front Froude number Fr_s and the rearward Froude number Fr_1), which indicate that the total momentum carried by the surge flow not only originates from the surge front, but also includes the contribution of surge-flow erosion into the deposition layer. The momentum ratios of surge flows at the Jiangjia Ravine exceed unity, indicating that it is not conservative to overlook the momentum concealed beneath the surge front in the risk assessment and mitigation of debris flows.

Conflict of Interest

The authors declare no conflicts of interest relevant to this study.

Data Availability Statement

The field observation data of 7 surge-flow events at the Jiangjia Ravine from 1999 to 2001 are obtained from the Dongchuan Debris Flow Observation and Research Station (DDFORS), Chinese Academy of Sciences, and they are available at the National Cryosphere Desert Data Center via https://doi.org/10.12072/DDFORS.024.2019.db with registration (Hong, 2016). The surge-depth hydrographs of 7 surge-flow events are available at Mountain Science Data Center via https://doi.org/10.12380/Debri.msdc.000012 with registration (Chen & Song, 2023). The movie of "pavement" of surge flows on 8 August 2023 at the Jiangjia Ravine is available at https://doi.org/10.12380/Debri.msdc.000020 (Chen & Song, 2024a). The movie of the downward erosion of surge flows on 2 August 2023 at the Jiangjia Ravine is available at https://doi.org/10.12380/Debri.msdc.000019 (Chen & Song, 2024b).

Acknowledgments

The authors acknowledge the financial supports from the National Natural Science Foundation of China (Grants 41925030. 42077256, and 42477193), National Cryosphere Desert Data Center (Grant E01Z790201), and the Science and Technology Research Program of Institute of Mountain Hazards and Environment, Chinese Academy of Sciences (Grants IMHE-CXTD-02 and IMHE-JCCX-02). We would like to thank the Dongchuan Debris Flow Observation and Research Station (DDFORS), Chinese Academy of Sciences, which provides the field observation data of the Jiangjia Ravine debris flows.

References

Aaron, J., Spielmann, R., McArdell, B. W., & Graf, C. (2023). High-frequency 3D LiDAR measurements of a debris flow: A novel method to investigate the dynamics of full-scale events in the field. *Geophysical Research Letters*, 50(5), e2022GL102373. https://doi.org/10.1029/2022GL102373

Ancey, C., & Cochard, S. (2009). The dam-break problem for Herschel–Bulkley viscoplastic fluids down steep flumes. *Journal of Non-Newtonian Fluid Mechanics*, 158(1–3), 18–35. https://doi.org/10.1016/j.jnnfm.2008.08.008

Arai, M., Huebl, J., & Kaitna, R. (2013). Occurrence conditions of roll waves for three grain-fluid models and comparison with results from experiments and field observation. *Geophysical Journal International*, 195(3), 1464–1480. https://doi.org/10.1093/gji/ggt352

Bartelt, P., Bühler, Y., Buser, O., Christen, M., & Meier, L. (2012). Modeling mass-dependent flow regime transitions to predict the stopping and depositional behavior of snow avalanches. *Journal of Geophysical Research*, 117(F1). https://doi.org/10.1029/2010JF001957

Bartelt, P., Buser, O., & Platzer, K. (2007). Starving avalanches: Frictional mechanisms at the tails of finite-sized mass movements. *Geophysical Research Letters*, 34(20). https://doi.org/10.1029/2007g1031352

Bates, B., & Ancey, C. (2017). The dam-break problem for eroding viscoplastic fluids. *Journal of Non-Newtonian Fluid Mechanics*, 243, 64–78. https://doi.org/10.1016/j.jnnfm.2017.01.009

Berezin, Y. A., Chugunov, V. A., & Hutter, K. (2001). Hydraulic jumps on shallow layers of non-Newtonian fluids. *Journal of Non-Newtonian Fluid Mechanics*, 101(1–3), 139–148. https://doi.org/10.1016/s0377-0257(01)00154-9

Berger, C., McArdell, B. W., & Schlunegger, F. (2011). Direct measurement of channel erosion by debris flows, Illgraben, Switzerland. *Journal of Geophysical Research*, 116(F1). https://doi.org/10.1029/2010JF001722

Briukhanov, A. V., Grigorian, S. S., Miagkov, S. M., Plam, M. Y., Shurova, I. Y., Eglit, M., & Yakimov, Y. L. (1967). On some new approaches to the dynamics of snow avalanches. *Physics of Snow and Ice: proceedings, 1*(2), 1223–1241. http://hdl.handle.net/2115/20373

Brown, R., & Chanson, H. (2012). Suspended sediment properties and suspended sediment flux estimates in an inundated urban environment during a major flood event. Water Resources Research, 48(11). https://doi.org/10.1029/2012WR012381

Capart, H., & Young, D. L. (1998). Formation of a jump by the dam-break wave over a granular bed. *Journal of Fluid Mechanics*, 372, 165–187. https://doi.org/10.1017/S0022112098002250

Chanson, H. (2004). 4 - Applications of the momentum principle: Hydraulic jump, surge and flow resistance in open channels. In H. Chanson (Ed.), *Hydraulics of open channel flow* (2nd ed., pp. 50–93). Butterworth-Heinemann. https://doi.org/10.1016/B978-075065978-9/50009-X Chanson, H. (2012). Momentum considerations in hydraulic jumps and bores. *Journal of Irrigation and Drainage Engineering*, 138(4), 382–385.

https://doi.org/10.1061/(ASCE)IR.1943-4774.0000409

Chanson, H., Jarny, S., & Coussot, P. (2006). Dam break wave of thixotropic fluid. *Journal of Hydraulic Engineering*, 132(3), 280–293. https://doi.org/10.1061/(ASCE)0733-9429(2006)132:3(280)

CHEN ET AL. 18 of 21



- Chanson, H., Reungoat, D., Simon, B., & Lubin, P. (2011). High-frequency turbulence and suspended sediment concentration measurements in the Garonne River tidal bore. *Estuarine, Coastal and Shelf Science*, 95(2), 298–306. https://doi.org/10.1016/j.ecss.2011.09.012
- Chen, Q., & Song, D. (2023). Flow depth measured by ultrasonic sensors and kinematic elements of surge flows in Jiangjia Ravine [Dataset]. Dongchuan, Yunnan, China 1999-2001. https://doi.org/10.12380/Debri.msdc.000012
- Chen, Q., & Song, D. (2024a). The "pavement" of surge flows on August 8, 2023 at Jiangjia Ravine [Dataset]. https://doi.org/10.12380/Debri. msdc.000020
- Chen, Q., & Song, D. (2024b). The downward erosion of surge flows on August 2, 2023 at Jiangjia Ravine [Dataset]. https://doi.org/10.12380/ Debri.msdc.000019
- Chen, Q., Song, D., Chen, X., & Zhong, W. (2023). Visco-collisional scaling law of flow resistance and its application in debris-flow mobility. Journal of Geophysical Research: Earth Surface, 128(2), e2022JF006712. https://doi.org/10.1029/2022JF006712
- Coe, J., Kean, J., McCoy, S., Staley, D., & Wasklewicz, T. (2010). Chalk Creek Valley: Colorado's natural debris-flow laboratory. *Generations: Geologic and Anthropogenic Field Excursions in the Rocky Mountains from Modern to Ancient*, 95–117. https://doi.org/10.1130/2010.0018(05)
- Comiti, F., Marchi, L., Macconi, P., Arattano, M., Bertoldi, G., Borga, M., et al. (2014). A new monitoring station for debris flows in the European Alps: First observations in the Gadria basin. *Natural Hazards*, 73(3), 1175–1198. https://doi.org/10.1007/s11069-014-1088-5
- Coussot, P. (1995). Structural similarity and transition from Newtonian to non-Newtonian behavior for clay-water suspensions. *Physical Review Letters*, 74(20), 3971–3974. https://doi.org/10.1103/PhysRevLett.74.3971
- Coussot, P., Nguyen, Q. D., Huynh, H. T., & Bonn, D. (2002). Avalanche behavior in yield stress fluids. *Physical Review Letters*, 88(17), 175501. https://doi.org/10.1103/PhysRevLett.88.175501
- Coussot, P., & Ovarlez, G. (2010). Physical origin of shear-banding in jammed systems. *The European Physical Journal E*, 33(3), 183–188. https://doi.org/10.1140/epje/i2010-10660-9
- Coussot, P., Roussel, N., Jarny, S., & Chanson, H. (2005). Continuous or catastrophic solid-liquid transition in jammed systems. *Physics of Fluids*, 17(1), 11–33. https://doi.org/10.1063/1.1823531
- Cui, P., Chen, X., Waqng, Y., Hu, K., & Li, Y. (2005). Jiangjia Ravine debris flows in south-western China. In P. Cui, X. Chen, Y. Waqng, K. Hu, & Y. Li (Eds.), Debris-flow hazards and related phenomena (pp. 565–594). Springer. https://doi.org/10.1007/3-540-27129-5_22
- Davies, T. R. H. (1986). Large debris flows: A macro-viscous phenomenon. Acta Mechanica, 63(1), 161–178. https://doi.org/10.1007/BF01182546
- Davies, T. R. H., Phillips, C., Pearce, A., & Zhang, X. (1992). Debris flow behaviour An integrated overview (Vol. 209). IAHS Publ. Retrieved from https://iahs.info/uploads/dms/9009.217-225-209-Davies.pdf
- Di Cristo, C., Iervolino, M., Vacca, A., & Zanuttigh, B. (2009). Roll-waves prediction in dense granular flows. *Journal of Hydrology*, 377(1–2), 50–58. https://doi.org/10.1016/j.jhydrol.2009.08.008
- Edwards, A. N., & Gray, J. (2015). Erosion-deposition waves in shallow granular free-surface flows. *Journal of Fluid Mechanics*, 762, 35–67. https://doi.org/10.1017/jfm.2014.643
- Edwards, A. N., Viroulet, S., Johnson, C. G., & Gray, J. (2021). Erosion-deposition dynamics and long distance propagation of granular avalanches. *Journal of Fluid Mechanics*, 915, A9. https://doi.org/10.1017/jfm.2021.34
- Eglit, M., Yakubenko, A., & Zayko, J. (2020). A review of Russian snow avalanche models—From analytical solutions to novel 3D models. Geosciences, 10(2), 77. https://doi.org/10.3390/geosciences10020077
- Faug, T. (2015). Depth-averaged analytic solutions for free-surface granular flows impacting rigid walls down inclines. *Physical Review E: Statistical, Nonlinear, and Soft Matter Physics, 6,* 062310. https://doi.org/10.1103/PhysRevE.92.062310
- Faug, T., Childs, P., Wyburn, E., & Einav, I. (2015). Standing jumps in shallow granular flows down smooth inclines. *Physics of Fluids*, 27(7), 073304. https://doi.org/10.1063/1.4927447
- Gray, J., & Cui, X. (2007). Weak, strong and detached oblique shocks in gravity-driven granular free-surface flows. *Journal of Fluid Mechanics*, 579, 113–136. https://doi.org/10.1017/S0022112007004843
- Guo, X., Li, Y., Cui, P., Yan, H., & Zhuang, J. (2020). Intermittent viscous debris flow formation in Jiangjia Gully from the perspectives of hydrological processes and material supply. *Journal of Hydrology*, 589, 125184. https://doi.org/10.1016/j.jhydrol.2020.125184
- Hofland, B., Kaminski, M., & Wolters, G. (2011). Large scale wave impacts on a vertical wall. Coastal Engineering Proceedings, (32), 15. https://doi.org/10.9753/icce.v32.structures.15
- Hong, Y. (2016). Movement elements and general observation statistics of debris flow in Jiangjia gully, Dongchuan, Yunnan, 1999-2005 [Dataset]. National Cryosphere Desert Data Center. https://doi.org/10.12072/DDFORS.024.2019.db
- Huang, B., Li, B., Zheng, J., Feng, W., Chen, X., & Luo, C. (2022). Dynamic analysis of impulse waves generated by the collapse of granular pillars. *Journal of Mountain Science*, 19(01), 198–210. https://doi.org/10.1007/s11629-020-6558-5
- Huebl, J., & Kaitna, R. (2021). Monitoring debris-flow surges and triggering rainfall at the Lattenbach Creek, Austria. *Environmental and Engineering Geoscience*, 27(2), 213–220. https://doi.org/10.2113/EEG-D-20-00010
- Ippen, A. T. (1951). High-velocity flow in open channels: A symposium: Mechanics of supercritical flow. *Transactions of the American Society of Civil Engineers*, 116(1), 268–295. https://doi.org/10.1061/TACEAT.0006520
- Iverson, R. M. (2012). Elementary theory of bed-sediment entrainment by debris flows and avalanches. *Journal of Geophysical Research*, 117(F3). https://doi.org/10.1029/2011JF002189
- Kang, Z. C., Lee, C. F., Ma, A. N., & Luo, J. T. (2004). Research on debris flow in China (pp. 213–224). Science Press. (in Chinese). Retrieved from http://ir.imde.ac.cn/handle/131551/3663
- Kean, J. W., Coe, J. A., Coviello, V., Smith, J. B., McCoy, S. W., & Arattano, M. (2015). Estimating rates of debris flow entrainment from ground vibrations. Geophysical Research Letters, 42(15), 6365–6372. https://doi.org/10.1002/2015GL064811
- Kean, J. W., McCoy, S. W., Tucker, G. E., Staley, D. M., & Coe, J. A. (2013). Runoff-generated debris flows: Observations and modeling of surge initiation, magnitude, and frequency. *Journal of Geophysical Research: Earth Surface*, 118(4), 2190–2207. https://doi.org/10.1002/jgrf.20148
- Khanfouf, O., Fatima Zohra, F., Fourar, A., Massouh, F., Rachid, C., Zeroual, A., & Khelladi, S. (2022). Influence of model selection on the temperature field and turbulent energy dissipation rate in a hydraulic system with a complex geometry. *Modeling Earth Systems and Environment*, 9(2), 2125–2139. https://doi.org/10.1007/s40808-022-01591-4
- Khezri, N., & Chanson, H. (2012). Inception of bed load motion beneath a bore. Geomorphology, 153–154, 39–47. https://doi.org/10.1016/j.geomorph.2012.02.006
- Leal, J., Ferreira, R., & Cardoso, A. (2006). Dam-break wave-front celerity. *Journal of Hydraulic Engineering-asce*, 132(1), 132–176. https://doi.org/10.1061/(ASCE)0733-9429(2006)132:1(69)
- Leng, X., & Chanson, H. (2017). Upstream propagation of surges and bores: Free-surface observations. Coastal Engineering Journal, 59(1), 1750003-1-1750003-32. 1750003-1750000-1750000-1750000-1750000-1750000-1750000-1750000-1750000-1750000-1750000-175000-1750000-175000-17

CHEN ET AL. 19 of 21



- Li, J., Y, J. M., Bi, C., & Luo, D. F. (1983). The main features of the mudflow in Jiang-Jia Ravine. Zeitschrift Fur Geomorphologie, 27(3), 325–341. https://doi.org/10.1127/zfg/27/1983/325
- Lugni, C., Brocchini, M., & Faltinsen, O. M. (2006). Wave impact loads: The role of the flip-through. Physics of Fluids, 18(12). https://doi.org/10.1063/1.2399077
- Major, J. J., Pierson, T. C., & Scott, K. M. (2005). Debris flows at Mount St. Helens, Washington, USA. In Debris-flow hazards and related phenomena (pp. 685–731). https://doi.org/10.1007/3-540-27129-5_27
- Marchi, L., Arattano, M., & Deganutti, A. M. (2002). Ten years of debris-flow monitoring in the Moscardo Torrent (Italian Alps). Geomorphology, 46(1-2), 1-17. https://doi.org/10.1016/s0169-555x(01)00162-3
- McArdell, B. W., Bartelt, P., & Kowalski, J. (2007). Field observations of basal forces and fluid pore pressure in a debris flow. *Geophysical Research Letters*, 34(7). https://doi.org/10.1029/2006GL029183
- McCoy, S., Kean, J. W., Coe, J. A., Tucker, G., Staley, D. M., & Wasklewicz, T. (2012). Sediment entrainment by debris flows: In situ measurements from the headwaters of a steep catchment. *Journal of Geophysical Research*, 117(F3). https://doi.org/10.1029/2011JF002278
- Mejean, S., Faug, T., & Einav, I. (2017). A general relation for standing normal jumps in both hydraulic and dry granular flows. *Journal of Fluid Mechanics*, 816, 331–351. https://doi.org/10.1017/jfm.2017.82
- Méjean, S., Guillard, F., Faug, T., & Einav, I. (2020). Length of standing jumps along granular flows down smooth inclines. *Physical Review Fluids*, 5(3), 034303. https://doi.org/10.1103/PhysRevFluids.5.034303
- Molnár, P., & Ramírez, J. A. (1998). Energy dissipation theories and optimal channel characteristics of river networks. *Water Resources Research*, 34(7), 1809–1818. https://doi.org/10.1029/98WR00983
- Nagl, G., Hübl, J., & Kaitna, R. (2020). Velocity profiles and basal stresses in natural debris flows. *Earth Surface Processes and Landforms*, 45(8), 1764–1776. https://doi.org/10.1002/esp.4844
- Nanson, G. C., & Huang, H. Q. (2008). Least action principle, equilibrium states, iterative adjustment and the stability of alluvial channels. *Earth Surface Processes and Landforms*, 33(6), 923–942. https://doi.org/10.1002/esp.1584
- Nanson, G. C., & Huang, H. Q. (2018). A philosophy of rivers: Equilibrium states, channel evolution, teleomatic change and least action principle. Geomorphology, 302, 3–19. https://doi.org/10.1016/j.geomorph.2016.07.024
- Ng, C. W. W., Jia, Z., Poudyal, S., Bhatta, A., & Liu, H. (2023). Two-phase MPM modelling of debris flow impact against dual rigid barriers. Géotechnique, 74(12), 1–14. https://doi.org/10.1680/igeot.22.00199
- Peregrine, D. H. (2003). Water-Wave impact on walls. Annual Review of Fluid Mechanics, 35(1), 23–43. https://doi.org/10.1146/annurev.fluid. 35.101101.161153
- Pouliquen, O. (1999). Scaling laws in granular flows down rough inclined planes. *Physics of Fluids*, 11(3), 542–548. https://doi.org/10.1063/1. 869928
- Pudasaini, S., & Fischer, J.-T. (2016). A mechanical erosion model for two-phase mass flows. *International Journal of Multiphase Flow*, 132, 103416. https://doi.org/10.1016/j.ijmultiphaseflow.2020.103416
- Razis, D., Edwards, A. N., Gray, J., & van der Weele, K. (2014). Arrested coarsening of granular roll waves. *Physics of Fluids*, 26(12). https://doi.org/10.1063/1.4904520
- Reungoat, D., Leng, X., & Chanson, H. (2017). Successive impact of tidal bores on sedimentary processes: Arcins channel, Garonne River. Estuarine, Coastal and Shelf Science, 188, 163–173. https://doi.org/10.1016/j.ecss.2017.02.025
- Rocha, F. M., Johnson, C. G., & Gray, J. (2019). Self-channelisation and levee formation in monodisperse granular flows. *Journal of Fluid Mechanics*, 876, 591–641. https://doi.org/10.1017/jfm.2019.518
- Rouse, H. (1938). Fluid mechanics for hydraulic engineers. McGraw-Hill Book Co. Retrieved from http://catalog.hathitrust.org/api/volumes/oclc/1709717.html
- Slepyan, L. (1993). Principle of maximum energy dissipation rate in crack dynamics. *Journal of the Mechanics and Physics of Solids*, 41(6), 1019–1033. https://doi.org/10.1016/0022-5096(93)90053-I
- Song, D., Bai, Y. T., Chen, X. Q., Choi, C. E., Pasuto, A., & Peng, P. (2022). Assessment of debris flow multiple-surge load model based on the physical process of debris-barrier interaction. *Landslides*, 19(5), 1165–1177. https://doi.org/10.1007/s10346-021-01778-3
- Song, D., Chen, X., Sadeghi, H., Zhong, W., Hu, H., & Liu, W. (2023). Impact behavior of dense debris flows regulated by pore-pressure feedback. *Journal of Geophysical Research: Earth Surface*, 128(12), e2023JF007074. https://doi.org/10.1029/2023JF007074
- Song, D., Chen, X. Q., Zhou, G. G. D., Lu, X. Q., Cheng, G. W., & Chen, Q. (2021). Impact dynamics of debris flow against rigid obstacle in laboratory experiments. *Engineering Geology*, 291, 106211. https://doi.org/10.1016/j.enggeo.2021.106211
- Sovilla, B., & Bartelt, P. (2002). Observations and modelling of snow avalanche entrainment. *Natural Hazards and Earth System Sciences*, 2(3–4), 169–179. https://doi.org/10.5194/nhess-2-169-2002
- Spinewine, B., & Zech, Y. (2007). Small-scale laboratory dam-break waves on movable beds. *Journal of Hydraulic Research*, 45(sup1), 73–86. https://doi.org/10.1080/00221686.2007.9521834
- Stoker, J. J. (1957). Water waves; the mathematical theory with applications. Interscience Publishers. https://doi.org/10.3233/SAV-1995-2108
 Takagi, D., McElwaine, J. N., & Huppert, H. E. (2011). Shallow granular flows. Physical Review E, 83(3), 031306. https://doi.org/10.1103/PhysRevE.83.031306
- Tranmer, A. W., Caamaño, D., & Goodwin, P. (2020). Identifying dynamic equilibrium of an undeveloped alluvial stream by extremal hypotheses. *Catena*, 194, 104680. https://doi.org/10.1016/j.catena.2020.104680
- Ugarelli, R., & Di Federico, V. (2007). Transition from supercritical to subcritical regime in free surface flow of yield stress fluids. *Geophysical Research Letters*, 34(21). https://doi.org/10.1029/2007GL031487
- Ulu, A., Aydin, M., & Önen, F. (2023). Energy dissipation potentials of grouped spur dikes in an open channel. *Water Resources Management*, 37(11), 1–16. https://doi.org/10.1007/s11269-023-03571-4
- Viroulet, S., Edwards, A. N., Johnson, C. G., Kokelaar, B. P., & Gray, J. M. N. T. (2019). Shedding dynamics and mass exchange by dry granular waves flowing over erodible beds. *Earth and Planetary Science Letters*, 523, 115700. https://doi.org/10.1016/j.epsl.2019.07.003
- Wan, Z., Wang, Z., & Julien, P. Y. (1994). Hyperconcentrated flow. *Journal of Hydraulic Engineering*, 120(10), 1234. https://doi.org/10.1061/(ASCE)0733-9429(1994)120:10(1234)
- Wu, J. S., Kang, Z. C., Q, T. L., & Zhang, S. C. (1990). Research and observation of debris flows in Jiangjia Gully, Yunnan. Science Press. (in Chinese). Retrieved from http://ir.imde.ac.cn/handle/131551/3847
- Wu, J. S., Zhang, J., Cheng, C. L., You, Y., & Diao, H. F. (2003a). Relation and its determination of residual layer and depth of viscous debris flow. *Journal of Sediment Research*, (06), 7–12. (in Chinese). https://doi.org/10.16239/j.cnki.0468-155x.2003.06.002
- Wu, J. S., Zhang, J., Cheng, C. L., You, Y., & Diao, H. F. (2003b). Relationship between depth and residual layer of viscous debris flow. *Journal of Mountain Science*, 21(04), 487–492. (in Chinese). Retrieved from http://shandixb.paperonce.org/oa/DArticle.aspx?type=view&id=200384

CHEN ET AL. 20 of 21





- Yalin, M. S., & Ferreira Da Silva, A. M. (1999). Regime channels in cohesionless alluvium. *Journal of Hydraulic Research*, 37(6), 725–742. https://doi.org/10.1080/00221689909498508
- Zanuttigh, B., & Lamberti, A. (2007). Instability and surge development in debris flows. *Reviews of Geophysics*, 45(3). https://doi.org/10.1029/2005rg000175
- Zech, Y., Soares-Frazão, S., Spinewine, B., & Le Grelle, N. (2008). Dam-break induced sediment movement: Experimental approaches and numerical modelling. *Journal of Hydraulic Research*, 46(2), 176–190. https://doi.org/10.1080/00221686.2008.9521854
- Zhang, J., Wu, J. S., You, Y., & Cheng, Z. L. (2003). Formation of residue layer of debris flow and the reduction of resistance. *Journal of Mountain Science*(02), 223–227. (in Chinese). Retrieved from http://shandixb.paperonce.org/oa/DArticle.aspx?type=view&id=200334
- Zhao, T., Zhou, G. G. D., Sun, Q., Crosta, G. B., & Song, D. (2022). Slope erosion induced by surges of debris flow: Insights from field experiments. *Landslides*, 19(10), 2367–2377. https://doi.org/10.1007/s10346-022-01914-7

CHEN ET AL. 21 of 21